Structural and electrical characterisation of Nb^{5+} and Cr^{6+} substituted La$_2$Mo$_2$O$_9$

D. MARRERO-LÓPEZ[1,*], J. PEÑA-MARTÍNEZ[1], J. C. RUIZ-MORALES[1], D. PÉREZ-COLL[1], M. C. MARTÍN-SEDEÑO[2], P. NÚÑEZ[1]

[1]Department of Inorganic Chemistry, University of La Laguna, 38200-La Laguna, Tenerife, Spain.
[2]Department of Inorganic Chemistry, University of Malaga, 29071-Malaga, Spain.

La$_2$Mo$_{2-y}$B$_y$O$_{9-\delta}$ (B=Cr and Nb) series have been prepared as nanocrystalline materials from a freeze-drying precursor method. The structural characterisation and stabilisation of the high temperature β-polymorph were investigated by high resolution X-ray diffraction (XRD) and differential scanning calorimetry (DSC). The overall conductivity was studied by impedance spectroscopy in the temperature range of 200-800ºC. Nb has a solubility limit of y<0.1 in La$_2$Mo$_2$O$_9$, stabilising the β-polymorph at room temperature. On the other hand, Mo can be partially substituted by Cr up to y=1 and it also stabilises the β-polymorph. These substitutions do not improve the ionic conductivity compared to non-substituted La$_2$Mo$_2$O$_9$. Only the sample with highest Cr-content showed a significant enhancement of the overall conductivity, which seems to be explained by an increase of the electronic contribution due to Cr reduction.

Keywords: La$_2$Mo$_2$O$_9$, solid electrolyte, phase transition.

Caracterización estructural y eléctrica del La$_2$Mo$_2$O$_9$ substituido por Nb^{5+} y Cr^{6+}

La serie de compuestos La$_2$Mo$_{2-y}$B$_y$O$_{9-\delta}$ (B=Cr and Nb) ha sido preparada en forma de materiales nanocristalinos a partir de un método de precursores liofilizados. La caracterización estructural y estabilización del polimorfo-β de alta temperatura fueron investigadas por difracción de rayos-X de alta resolución (XRD) y calorimetría diferencial de barrido (DSC). La conductividad total fue estudiada por espectroscopía de impedancia en el rango de temperaturas de 200-800ºC. El Nb tiene una solubilidad límite de solo y=0.1 en La$_2$Mo$_2$O$_9$ y estabiliza el polimorfo-β a temperatura ambiente. Por otra parte, el Mo puede ser parcialmente substituido por Cr hasta y=1 estabilizando también el polimorfo-β. Estas sustituciones no mejoran la conductividad iónica de la fase original La$_2$Mo$_2$O$_9$. Únicamente la muestra con mayor contenido en Cr mostró un aumento significativo de la conductividad, el cual parece ser explicado por un incremento de la contribución electrónica debido a la reducción del Cr.

Palabras clave: La$_2$Mo$_2$O$_9$, electrolito sólido, transición de fase.

1. INTRODUCTION

La$_2$Mo$_2$O$_9$ based materials (LAMOX) have been studied in last few years as potential solid electrolytes for intermediate temperature applications, such as oxygen sensor, dense membranes for oxygen separation and electrolyte for solid oxide fuel cells (SOFCs) (1,2). Non-substituted La$_2$Mo$_2$O$_9$ phase presents two different polymorphs with a reversible structural phase transition at 560ºC, which is accompanied with a great improvement of the ionic conductivity above the phase transition temperature. The low temperature α-polymorph shows a 2×3×4 superstructure relative to the high temperature and better conductor cubic β-polymorph, which is usually associated to a rearrangement in the oxygen sublattice (3-6). The phase transition of non-substituted La$_2$Mo$_2$O$_9$ is detrimental for practical applications due to a drastic drop in the conductivity below 560ºC and mechanical failure caused by the high thermal expansion between the high and low temperature polymorphs. A doping strategy has been investigated in order to stabilise the high temperature β-polymorph. In this sense, several series of compounds have been studied, substituting La^{3+} by Ca^{2+}, Ba^{2+}, Sr^{2+}, rare earth elements, etc. (7,8), whereas Mo^{6+} has been substituted by Cr^{6+}, V^{5+}, Nb^{5+} and W^{6+} (5, 9-11). These substitutions stabilise the β-structure at room temperature suppressing the phase transition to the α-form, with the exception of Nb and some rare-earth elements. On the other hand, some contradictions appear in the literature, regarding the effect of such substitutions on the overall conductivity, resulting from the different synthetic methods used and relative density of the samples studied (12). Furthermore, the β-La$_2$Mo$_2$O$_9$ exhibits also a limited stability range under reducing conditions due to the presence of Mo^{6+}, which is partially reduced causing an enhancement of the non-desirable n-type electronic conductivity and phase decomposition (13,14). One of the most promising substitution is W^{6+} replacing Mo^{6+}, because it enhances the phase stability under reducing

conditions, preserving the high ionic conductivity (typically 0.1 S/cm at 750ºC) (14,15). The better redox stability of $La_2Mo_{2-y}W_yO_9$ series seems to be explained by the lower reducibility of W^{6+} in comparison to Mo^{6+}. Indeed, XPS studies revealed that tungsten is not reduced during the phase decomposition under highly reducing conditions (16,17). Thus substitution of Mo^{6+} by adequate elements in $La_2Mo_2O_9$ could improve the phase stability under reducing conditions.

In the present work, the effects of Cr^{6+} and Nb^{5+} substitutions on the structure and transport properties of $La_2Mo_2O_9$ are studied. Some differences have been found in comparison to previous reports. For instance, the Nb solubility in $La_2Mo_2O_9$ is lower and the stabilisation of the β-polymorph is achieved at room temperature after Nb substitution. Additionally, the high conductivity previously observed for La_2MoCrO_9 sample seems to be due to reduction of Cr during the synthesis process, leading to a significant electronic contribution in the low temperature range.

2. EXPERIMENTAL

2.1 Synthesis

Polycrystalline powders of $La_2Mo_{2-y}B_yO_{9-\delta}$ (B=Cr and Nb) phases were prepared by a modified freeze-dried precursor method, similar to that previously described (18). La_2O_3 (99.9%, Aldrich), MoO_3 (99.9%, Aldrich), CrO_3 (99%, Aldrich) and $NbCl_5$ (99.5%, Aldrich) were used as starting materials. Stoichiometric amounts of La_2O_3 and MoO_3 were dissolved in diluted nitric acid and diluted ammonia, respectively, whereas CrO_3 was dissolved in distilled water. Ethylenediaminetetraacetic acid (EDTA) (99.5% Aldrich) solution was added as complexing agent in a ligand:metal molar ratio of 1:1.

Niobium chloride was dissolved separately in ethanol and then EDTA and ammonia solutions were added. This solution with a Nb:EDTA ratio of 1:1 was slowly heated in a hot-plate with continuous stirring to evaporate the ethanol, obtaining finally a clear transparent solution with pH=7. These solutions were mixed in stoichiometric amounts and then the pH was adjusted to 9 by adding ammonia. The volume and La^{3+}-cation concentration in a typical preparation were 200 ml and 0.15 M respectively. The solutions were frozen in liquid nitrogen and the resulting ice crystals were dehydrated in a Heto Lyolab freeze-dryer for 3 days. The dried and amorphous precursor powders obtained were initially precalcined at 300ºC to produce the pirolysis of the organic matter and then calcined at 550ºC for 5 h to remove the residual organic species and achieve crystallization of the compounds. The samples are hereafter labelled as LMO and B_y for undoped $La_2Mo_2O_9$ and $La_2Mo_{2-y}B_yO_{9-\delta}$ (B=Cr, Nb) series, respectively.

2.2 Characterisation

High-resolution X-ray diffraction (XRD) patterns were recorded using a PANanalytical X´Pert Pro diffractometer, equipped with a Ge(111) primary monochromator and X´celerator detector. The scans were collected in the 2θ range (5-100º) with 0.016º step for 2h. Structure refinements were performed using the FullProf and WinPlotr softwares (19).

Differential scanning calorimetry (DSC) curves were recorded with a Perkin Elmer Instrument (mod. Pyris Diamond), between 25 and 650ºC at a heating rate of 10 K·min⁻¹ in air atmosphere.

The morphology of sintered pellets was monitored using a scanning electron microscope (SEM) (mod. Jeol LTD, JSM-6300). All preparations were covered with a thin film of sputtered gold for better image definition.

X-ray photoelectron spectroscopy (XPS) measurements were carried on a Physical Electronics PHI-5700 spectrometer. The experimental peaks were decomposed into components using mixed Gaussian-Lorentzian functions using PHI ACCES ESCA-V6.0 F software.

Ceramic pellets were prepared by pressing the fine oxide powders obtained at 550ºC into disks of 10 mm of diameter and 1.5-2 mm of thickness at 125 MPa. The resulting pellets were sintered in air at 700ºC for Cr-substituted samples and 1100-1300ºC for Nb-substituted samples during 3 h. Pt-paste electrodes were painted symmetrically on each side of the pellet surfaces and then fired at 700-950ºC for 30 min to secure a good electrical connection with the electrochemical cell. Impedance spectra were collected on a 1260 Solartron Impedance Analyser in static air in the 0.1 Hz to 1 MHz frequency range from 800 to 250ºC. The cooling rate and stabilisation time between consecutive measurements were 5ºC·min⁻¹ and 15 min respectively. An ac signal of 25 mV was applied in the high temperature range (800-500ºC) and 100 mV in the low temperature range (500-250ºC). Data were analysed with equivalent circuits using ZView software (Scribner Associates 2002), which allows an estimation of the resistance and capacitance associated to the different contributions of the overall conductivity.

3. RESULTS AND DISCUSSIONS

3.1 Structure and phase stability

The XRD patterns for Cr-substituted $La_2Mo_2O_9$ samples are shown in Fig.1a after calcined at 700ºC for 5h. At this temperature $La_2Mo_{2-y}Cr_yO_9$ samples are single phases up to y=1 and above this concentration a secondary phase appears identified as the perovskite structure of $LaCrO_3$. The high resolution XRD patterns confirmed that the small peaks splitting due to the slight monoclinic distortion and additional small superstructure reflections associated to the low temperature α-polymorph disappear after Cr-substitution (inset Fig. 1a). In addition, the DSC curves did not show any thermal effect between room temperature and 700ºC for Cr-substituted samples. Thus, the β-polymorph is stabilised at room temperature for Cr-substitution levels of y≥0.25. It should be comment that these phases exhibit low stability above 700ºC due to complete reduction of Cr^{6+} to Cr^{3+}, appearing impurities of $LaCrO_3$. Note that this effect has not been taken into account in previous works (5,11).

The powders of Nb-substituted samples ($La_2Mo_{2-y}Nb_yO_{9-\delta}$) were pressed into pellets and calcined in a range of temperatures between 950 and 1300ºC for 3h and then ground and further characterised. The samples sintered at 950ºC show a significant fraction of a secondary phase identified as $LaNbO_4$, although the content of this secondary phase decreases as the firing temperature increases. This result indicates that samples containing Nb requires high sintering temperature to obtain a solid solution, nevertheless small secondary phases were found above y=0.1 at 1300ºC (Fig. 1b). Therefore, the solubility limit of Nb in $La_2Mo_2O_9$ found in the present work is relatively low (y<0.1) in comparison to a previous reports (9,10). Basu
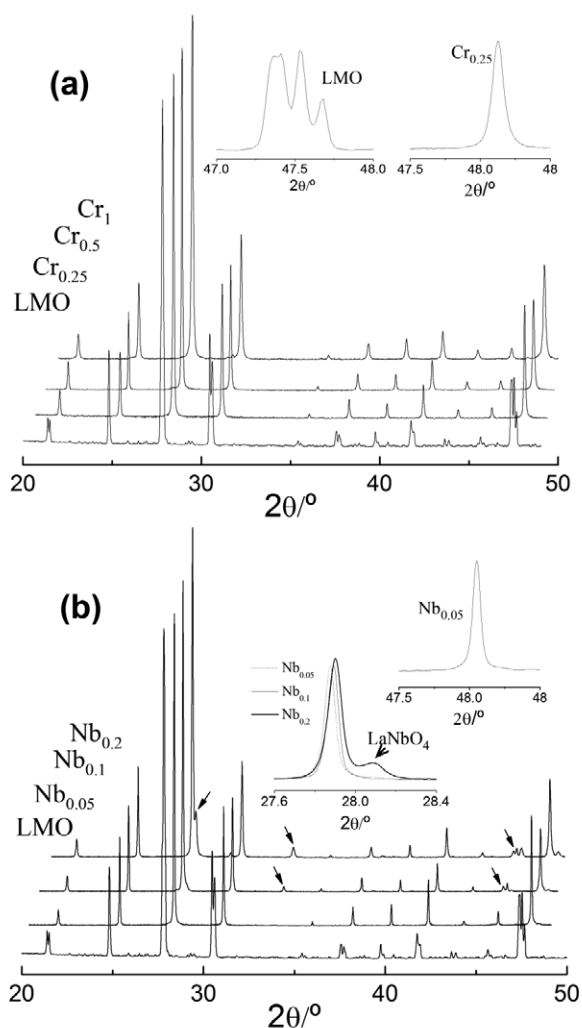
214

Bol. Soc. Esp. Ceram. V., 47, 4, 213-218 (2008)

Fig. 1- XRD patterns of (a) $La_2Mo_{2-y}Cr_yO_{9-\delta}$ (Cr_y) and (b) $La_2Mo_{2-y}Nb_yO_{9-\delta}$ (Nb_y) series calcined at 700 and 1300ºC respectively. Some impurity peaks appear for Niobium composition y≥0.1. The insets show the details of some XRD peaks.

Fig. 2- (a) Evolution of the (231) XRD peak and (b) DSC curves for $Nb_{0.1}$ sample as a function of the sintering temperature. The XRD peaks were shifted for better visualization.

et al. have reported that Mo can be substituted by Nb up to y<0.4, whereas Khadasheva et al. (10) reported a lower solubility value of y≤0.2. They also indicated that the phase transition is not completely suppressed after Nb substitution, observing that the phase transition peak in the DSC curves shifts to lower temperature as the Nb content increases and additionally the phase transition enthalpy decreases.

A zoom on the (231) XRD reflection for $Nb_{0.1}$ sample (Fig. 2a) show peak splitting at sintering temperatures below 1200ºC, which is characteristic of the monoclinic distortion of the low temperature α-polymorph. As the temperature increases the peak splitting disappear and a decrease of the XRD peak width is observed. This behaviour seems to indicate that the solubility of Nb into $La_2Mo_2O_9$ phase increases gradually with the firing temperature, stabilising the β-polymorph. A similar trend has been observed in Nd-substituted $La_2Mo_2O_9$ samples as the Nd content increases (5). On the other hand, the phase transition peak in the DSC curves is shifted to lower temperature as the firing temperature increases and the enthalpy change is gradually lowered and no phase transformation is detected after calcined at 1300ºC (Fig. 2b). These results seem to indicate that the cubic β-polymorph is
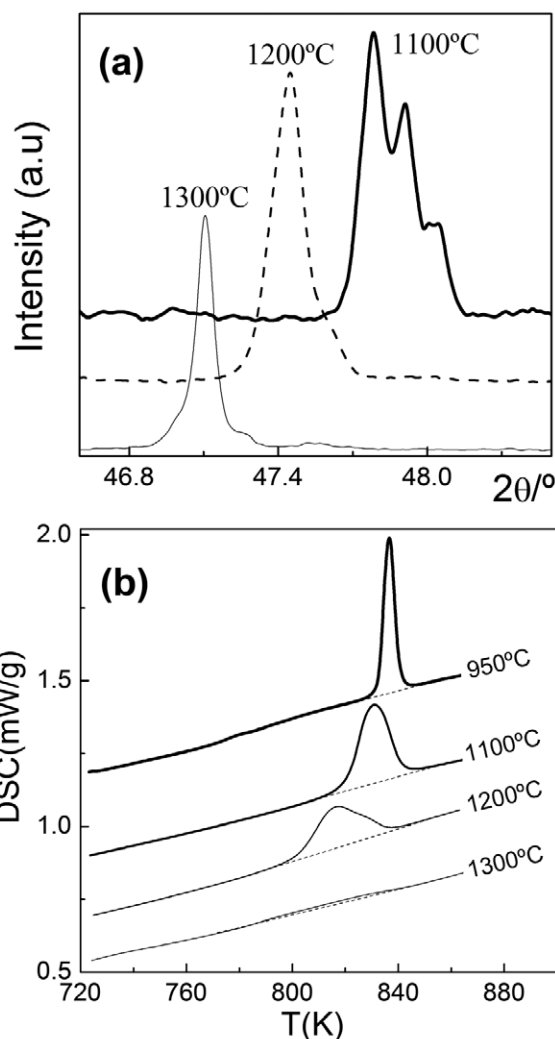
stabilised at room temperature when Nb⁵⁺ replaces partially Mo⁶⁺ and the calcining temperature is sufficiently high (1300ºC). Therefore, the discrepancies with previous reports can be explained by the different preparation method and sintering temperatures used.

The lattice cell variation with the dopant content (Cr, Nb, W) is shown in Fig. 3. For Cr substitutions the cell parameter decreases almost linearly with the dopant content up to y=0.5 in agreement with the smaller ionic radii of Cr⁶⁺ (0.44 Å) compared to Mo⁶⁺ (0.59 Å). However, a deviation of the Vegard´s law is observed for y>0.5. Note that samples with chromium content y<1 are yellow colour, whiles that for y=1 is slightly greenish, indicating a possible change in the oxidation state of chromium without phase change. Thus, the partial reduction of Cr⁶⁺ (0.44 Å) to lower oxidation state with larger ionic radii, i.e. Cr⁵⁺ (0.49 Å), might produce a slight expansion of the lattice unit cell compared to the expected value. This point has been further confirmed by XPS measurements. High resolution Cr2p spectrum (inset Fig. 3) shows a doublet ($Cr2p_{3/2}$ and $Cr2p_{1/2}$) with asymmetrical peaks. These peaks were decomposed into two components with binding energy (BE) values around 579.4 and 577.5 eV for the case of $Cr2p_{1/2}$.
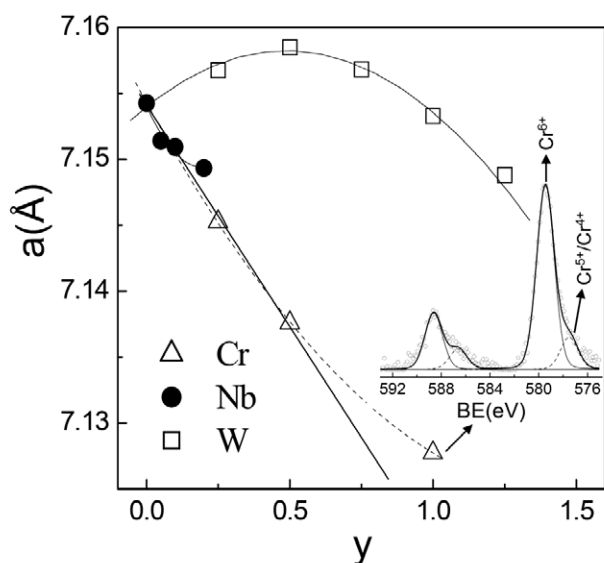
Bol. Soc. Esp. Ceram. V., 47, 4, 213-218 (2008)

215

Fig. 3- Variation of the lattice cell parameter for La$_2$Mo$_{2-y}$B$_y$O$_{9-\delta}$ (B=Cr, W, Nb) series as a function of the concentration of Cr, Nb and W. Samples were calcined at 700, 1100 and 1300ºC for Cr-, W- and Nb-containing samples, respectively. The inset shows the XPS Cr2p spectra for La$_2$MoCrO$_{9-\delta}$ (Cr$_1$) sample with two components assigned to Cr^{6+} and Cr^{5+}/Cr^{4+}.

The peak at 579.4 eV corresponds to Cr^{6+} (theoretical value of 579.5 eV), whereas the other component with binding energy of 577.5 eV could be assigned to both Cr^{5+} and/or Cr^{4+} cations with theoretical BE values of 578.0 and 576.9 eV, respectively. The presence of secondary phases in Cr$_1$ sample which could explain the deviation from the Vegard´s law is ruled out, because not additional diffraction peaks are observed by high resolution XRD.

The cell parameter variation for Nb-substituted series decreases slightly as the Nb content increases, which is contrary to the expected behaviour, because the ionic radii of Nb^{5+} (0.64 Å) is larger than Mo^{6+} (0.59 Å). A similar trend has been observed in W-substituted La$_2$Mo$_2$O$_9$ series (Fig. 3), where the cell parameter reach a maximum at y=0.5 decreasing for higher tungsten content. This behaviour was explained by a decrease in coordination number around W, although it should be noted that a slight distortion of the cubic cell was also observed for tungsten content y≤0.5 from both high resolution XRD and electron diffraction studies (5). One should also comment that the high sintering temperature used in the present work could produce a deviation in the cation stoichiometry of La$_2$Mo$_2$O$_9$ due to possible minor molybdenum volatilization as molybdenum oxide exhibits low melting temperature of 800ºC. This might affect the structure and phase transition behaviour. However, different samples were calcined at 1300ºC between 30 min and 3 h and the XRD patterns and lattice cell parameters were similar, without appreciable structural changes, nevertheless one can not rule out a possible volatilization of molybdenum.

3.2 Ceramic microstructure

Representative SEM images of the sintered pellets are shown in Fig. 4. Non-substituted La$_2$Mo$_2$O$_9$ sintered at 950ºC presents relative density higher than 98% and average grain size of 5-10 μm. Nb contained samples sintered at 1300ºC exhibit relative density higher than 98%. Small grains are visible in the grain boundary region of these samples, which were identified as phase segregations of LaNbO$_4$. Cr-substituted samples were sintered at 700ºC for 5h due to chromium reduction above this temperature, having low relative density around 65%.
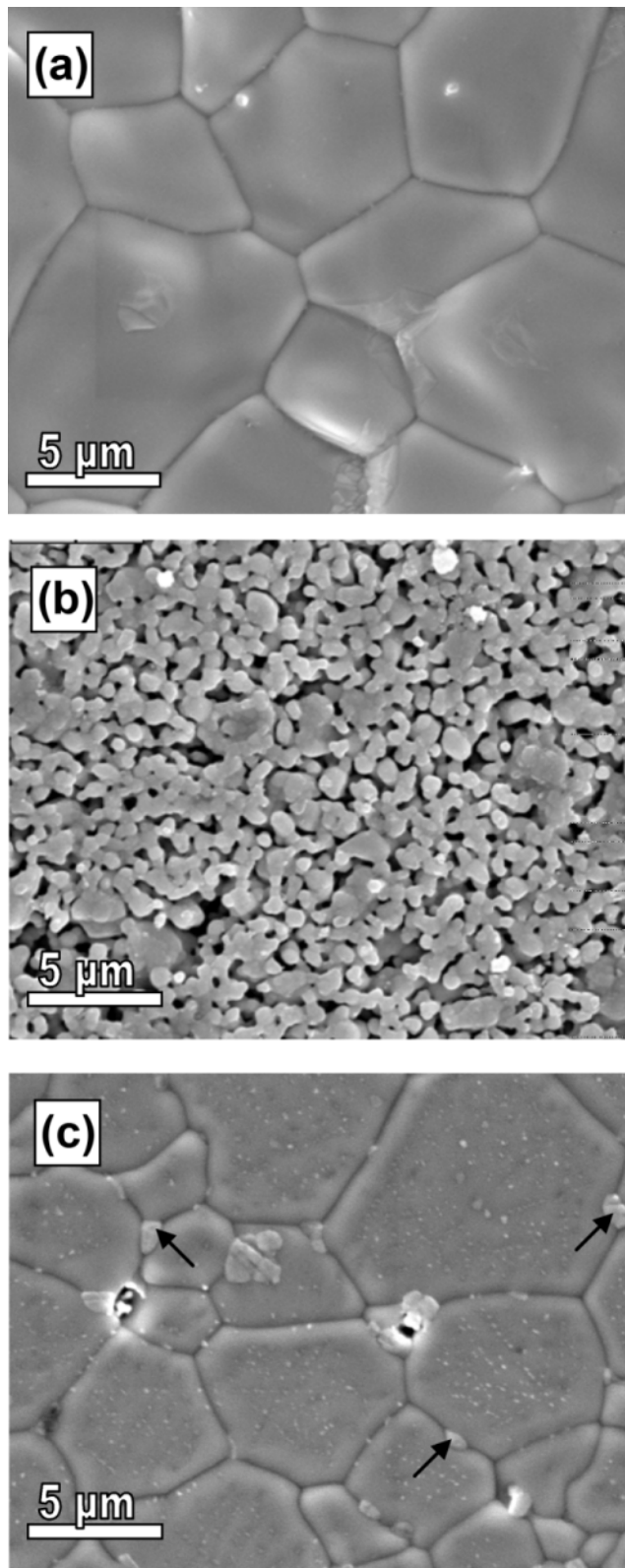

Fig. 4- SEM images for (a) La$_2$Mo$_2$O$_9$ sintered at 950ºC, (b) Cr01 sintered at 700ºC and (c) Nb01 sintered at 700ºC.

3.3 Electrical characterisation

Impedance spectra for $La_2Mo_2O_9$ samples were studied in a previous work (18) and only one electrolyte process ascribed to grain interior contribution was observed. Impedance spectra for Nb-substituted samples show an asymmetric and depressed arc in addition to electrode process at low frequency (Fig. 5a). These spectra were fitted with an equivalent circuit consisting in a series association of two (RQ) and one Q elements (inset Fig. 5a), where R is a resistance and Q is a pseudo-capacitance, which is related to the real capacitance C, as: $C=(Q)^{1/n}(R)^{(1-n)/n}$. The total circuit can thus be expressed as $(R_bQ_b)(R_{gb}Q_{gb})(Q_e)$, where the subscripts b, gb and e denote bulk, grain boundary and material/electrode processes respectively. These contributions have capacitance of ~5 pF·cm⁻¹ for grain interior (high frequency), ~1 nF·cm⁻¹ for grain boundary (intermediate frequency) and 0.2 mF·cm⁻¹ for electrode responses at low frequency. As can be observed, the grain boundary contribution is nearly negligible compared to bulk one. On the other hand, four different contributions are discernible in the impedance spectra of Cr-substituted samples (Fig. 5b). In this case, an equivalent circuit $(R_bQ_b)(R_{gb1}Q_{gb1})(R_{gb2}Q_{gb2})(Q_e)$ was used for fitting the spectra (inset Fig. 5b). The high frequency contribution with capacitance around 5 pF·cm⁻¹ is assigned to bulk. Two different contributions with similar capacitance values of 0.6 and 27 nF·cm⁻¹ are observed in the intermediate frequency range and they could be ascribed to internal interfaces (i.e. grain boundary, porosity and constrictions). These processes are derived from the low relative density of these samples ~65%. Finally the typical electrode response is observed at low frequency.
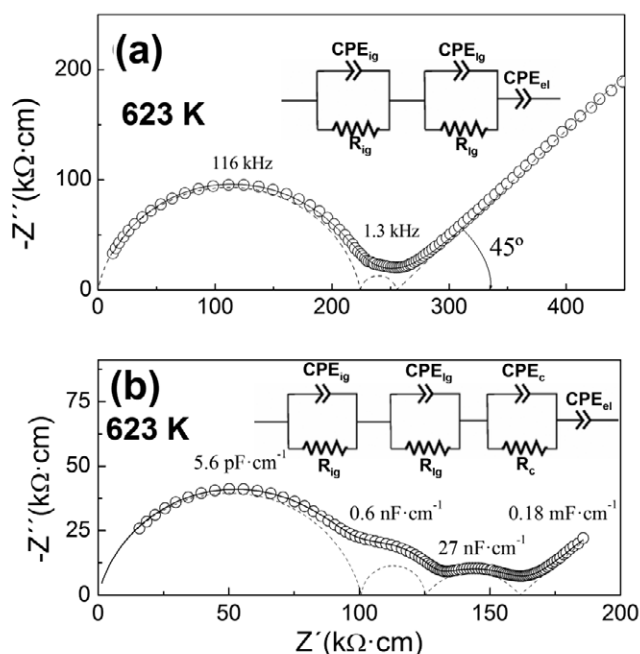
The Arrhenius plots of the overall conductivity are shown

in the intermediate temperature range. However, the conductivity in the high temperature range is somewhat lower compared to LMO (e.g. 0.08 S·cm⁻¹ for LMO and 0.051 S·cm⁻¹ for $Nb_{0.2}$ at 700ºC). Cr-substitution also suppresses the phase transition (Fig. 6b), but the conductivity decreases as the Cr content increases from y=0.25 to y=0.5. This is explained by the lower relative density of the ceramic samples as the Cr content increases, increasing the blocking effects in the internal interfaces. Additionally, the introduction of Cr produces a contraction of the cell volume limiting the free space for oxygen diffusion and consequently the conductivity is lower than for $La_2Mo_2O_9$. Surprisingly, the sample with highest Cr content (Cr_1) shows a significant improvement of the conductivity in the low temperature range. The same behaviour was previously observed by Goutenoire et al. [5], although an explanation was not given. The improvement of conductivity for Cr_1 sample could be related to the presence of reduced chromium, as observed by XPS, leading to a significant electron hopping conduction. The lower activation energy 0.56 eV for Cr_1 compared to 1.31 eV for $Cr_{0.5}$ seems to confirm this hypothesis.
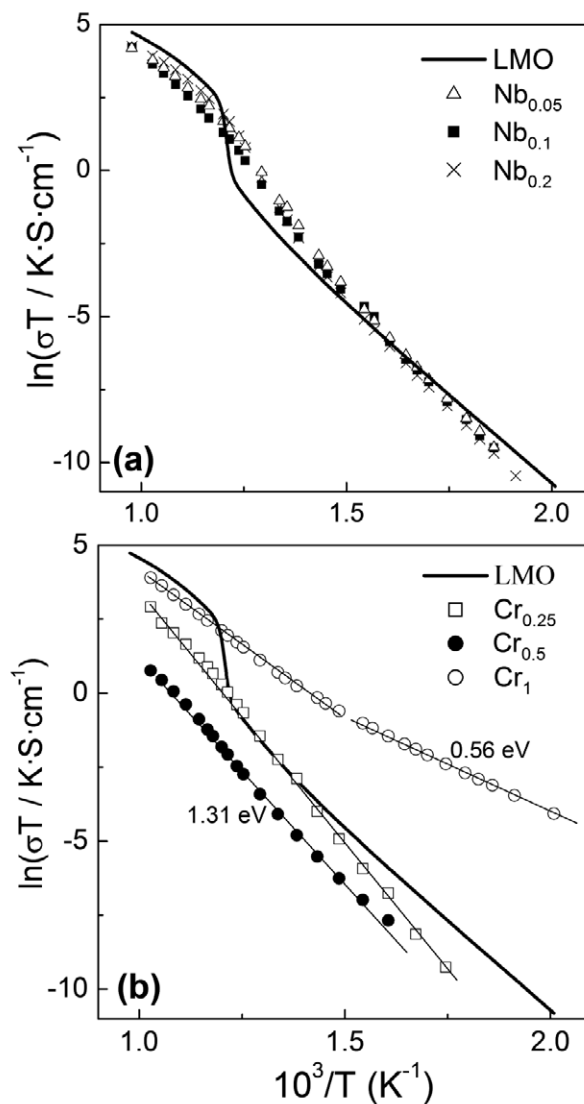

Fig. 5- Impedance spectra for (a) $Nb_{0.1}$ and (b) Cr_1 samples. The insets show the equivalent circuits used for fitting the impedance spectra (solid lines). The different contributions are also plotted separately for better visualisation (dashed lines).

in Fig. 6. The β®α phase transformation of non-substituted $La_2Mo_2O_9$ at 560ºC is accompanied by a significant increase of the conductivity. Such a phase transition is suppressed after Nb substitution (Fig. 6a), improving the overall conductivity

Fig. 6- Arrhenius plot of the overall conductivity for (a) $La_2Mo_{2-y}Nb_yO_{9-\delta}$ (Nb_y) and (b) $La_2Mo_{2-y}Cr_yO_{9-\delta}$ (Cr_y). For comparison, the conductivity of unsubstituted $La_2Mo_2O_9$ (LMO) is also plotted.

Bol. Soc. Esp. Ceram. V., 47, 4, 213-218 (2008)

217

In summary Nb and Cr substitution in $La_2Mo_2O_9$ stabilises the high temperature β-polymorph at room temperature. The solubility limit is approximately of 5% for Nb and 50% for Cr. Nb-content samples required high sintering temperature as 1300ºC to obtain a solid solution. On the other hand Cr-content samples present low phase stability above 700ºC due to chromium reduction. Moreover, these substitutions do not improve the conductivity in the high temperature range compared to non-substituted $La_2Mo_2O_9$.

ACKNOWLEDGEMENTS

BIBLIOGRAFÍA

1. N. Q. Minh and T. Takahashi, Science and Technology of Ceramic Fuel Cells, Elsevier Science, Amsterdam (Netherlands), pp. 1-15. (1995).
2. P. Lacorre, F. Goutenoire, O. Bohnke, R. Retoux, Designing fast oxide-ion conductors based on $La_2Mo_2O_9$, Nature, 404(6780), 856-858 (2000)
3. I. R. Evans, J. A. K. Howard, S. O. Evans, The crystal structure of α-$La_2Mo_2O_9$ and the structural origin of the oxide ion migration pathway, Chem. Mater. 17, 4074-4077 (2005).
4. F. Goutenoire, O. Isnard, R. Retoux and P. Lacorre, Crystal structure of $La_2Mo_2O_9$, a new fast oxide-ion conductor, Chem. Mater. 12(9), 2575-2580 (2000).
5. F. Goutenoire, O. Isnard, R. Retoux, O. Bohnke, Y. Laligant, P. Lacorre, Structural and transport characteristics of the LAMOX family of fast oxide-ion conductors, based on lanthanum molybdenum oxide $La_2Mo_2O_9$, J. Mater. Chem. 11(1), 119-124 (2001).
6. D. Marrero-López, J. Canales-Vazquez, W. Zhou, J. T. S. Irvine, P. Núñez, Structural studies on W^{6+} and Nd^{3+} substituted $La_2Mo_2O_9$ materials, J. Solid State Chem. 179(1), 278-288 (2006).
7. R. Subasri, D. Matusch, H. Näfe, F. Aldinger, Synthesis and characterization of $(La_{1-x}M_x)_2Mo_2O_{9-\delta}$; M=$Ca^{2+}$, Sr^{2+} or Ba^{2+}, J. Eur. Ceram. Soc. 24(1), 129-137 (2003).
8. D. Marrero-López, D. Pérez-Coll, J. C. Ruiz-Morales, J. Canales-Vázquez, M. C. Martín-Sedeño, P. Núñez, Synthesis and transport properties in $La_{2-x}A_xMo_2O_{9-\delta}$ (A=Ca^{2+}, Sr^{2+}, Ba^{2+}, K^+) series, Electrochim. Acta, 52(16), 5219-5231 (2007).
9. S. Basu, P. S. Devi, H. S. Maiti, Nb-doped $La_2Mo_2O_9$: A new materia wih high ionic conductivity, J. Electrochem. Soc. 152(11), A2143-A2147 (2005).
10. Z. S. Khadasheva, N. U. Venskovskii, M. G. Safronenko, A. V. Mosunov, E. D. Politova, S. Yu Stefanovich, Synthesis and properties of $La_2(Mo_{1-x}M_x)_2O_9$ (M = Nb, Ta) ionic conductors, Inorg. Mater. 38(11), 1168-1171 (2002).
11. Kwang Soo Yoo, Allan J. Jacobson, Effects of Sr and Cr doping on properties of $La_2Mo_2O_9$ electrolytes, J. Mater. Sc. 40(16), 4431-4434 (2005).
12. D. Marrero-López, J. Peña-Martínez, D. Pérez-Coll, P. Núñez, Effects of preparation method on the microstructure and transport properties of $La_2Mo_2O_9$ based materials, J. Alloys Compd. 422(1-2), 249-257 (2006).
13. D. Marrero-López, J. C. Ruiz-Morales, D. Pérez-Coll, P. Núñez, J. C. C. Abrantes, J. R. Frade, "Stability and transport properties of $La_2Mo_2O_9$, J. Solid State Electrochem. 8(9) 638-643 (2004).
14. S. Georges, F. Goutenoire, Y. Laligant, P. Lacorre, Reducibility of fast oxide-ion conductors $La_{2-x}R_xMo_{2-y}W_yO_9$ (R = Nd, Gd), J. Mater. Chem. 9, 2317-232 (2003).
15. D. Marrero-López, J. Canales-Vázquez, J. C. Ruiz-Morales, J. T. S. Irvine, P. Núñez, Electrical conductivity and redox stability of $La_2Mo_{2-x}W_xO_9$ materials, Electrochim. Acta, 50(22), 4385-4395 (2005).
16. Tsu-Yung Jin, M. V. Madhava Rao, Chia-Liang Cheng, Dah-Shyang Tsai, Ming-Hao Hung, Structural stability and ion conductivity of the Dy and W substituted $La_2Mo_2O_9$, Solid State Ionics, 178(5-6), 367-374 (2007).
17. D. Marrero-López, J. Peña-Martínez, J. C. Ruiz-Morales, D. Pérez-Coll, M. C. Martín-Sedeño, P. Núñez, Applicability of $La_2Mo_{2-y}W_yO_9$ materials as solid electrolyte for SOFCs, Solid State Ionics 178, 1366-1378 (2007).
18. D. Marrero-López, J. Canales-Vázquez, J.C. Ruiz-Morales, A. Rodríguez, J. T. S. Irvine, P. Núñez, Synthesis, sinterability and ionic conductivity of nanocrystalline $La_2Mo_2O_9$ powders, Solid State Ionics, 176(23-24), 1807-1816 (2005).
19. T. Roisnel, J. Rodríguez-Carvajal, WinPLOTR, a graphic tool for powder diffraction, Laboratoire Léon Brillouin-LCSI, France, (2005).

◆ ◆ ◆

218

Bol. Soc. Esp. Ceram. V., 47, 4, 213-218 (2008)